JVSTB
JOURNAL OF VACUUM SCIENCE AND TECHNOLOGY B

Native extended defects in Zn1−yCdySe/InxGa1−xAs heterostructures

B. Müller, S. Heun, R. Lantier, S. Rubini, J. J. Paggel et al.

Citation: J. Vac. Sci. Technol. B **16**, 2334 (1998); doi: 10.1116/1.590171
View online: http://dx.doi.org/10.1116/1.590171
View Table of Contents: http://avspublications.org/resource/1/JVTBD9/v16/i4
Published by the AVS: Science & Technology of Materials, Interfaces, and Processing

Related Articles

LOGISTIC FUNCTION PROFILE FIT: A least-squares program for fitting interface profiles to an extended logistic function
J. Vac. Sci. Technol. A 30, 051101 (2012)

Probing temporal evolution of extreme ultraviolet assisted contamination on Ru mirror by x-ray photoelectron spectroscopy
J. Vac. Sci. Technol. B 30, 021601 (2012)

Thermal-vacuum stability of the surface oxide complex on Cu
J. Vac. Sci. Technol. A 29, 053001 (2011)

Segregation and interlayer relaxation at the NiPd(111) surface
J. Vac. Sci. Technol. A 29, 011015 (2011)

Dose loss of phosphorus due to interface segregation in silicon-on-insulator substrates
J. Vac. Sci. Technol. B 28, 1158 (2010)

Additional information on J. Vac. Sci. Technol. B

Journal Homepage: http://avspublications.org/jvstb
Journal Information: http://avspublications.org/jvstb/about/about_the_journal
Top downloads: http://avspublications.org/jvstb/top_20_most_downloaded
Information for Authors: http://avspublications.org/jvstb/authors/information_for_contributors

ADVERTISEMENT

Native extended defects in $Zn_{1-y}Cd_ySe/In_xGa_{1-x}As$ heterostructures

B. Müller, S. Heun, R. Lantier, S. Rubini, J. J. Paggel,[a] L. Sorba,[b] A. Bonanni, M. Lazzarino, B. Bonanni, and A. Franciosi[c]
Laboratorio Nazionale TASC-INFM, Area di Ricerca, Padriciano 99, I-34012 Trieste, Italy

E. Napolitani, F. Romanato,[d] and A. Drigo
INFM and Dipartimento di Fisica, Universita' di Padova, I-35131 Padova, Italy

J.-M. Bonard and J.-D. Ganière
Institut de Micro- et Optoélectronique, Département de Physique, Ecole Polytechnique Fédérale, CH-1015 Lausanne, Switzerland

L. Lazzarini and G. Salviati
Istituto MASPEC del CNR, Parma, Italy

(Received 21 January 1998; accepted 11 May 1998)

Lattice-matched $Zn_{1-y}Cd_ySe/In_xGa_{1-x}As$ heterojunctions can be fabricated by molecular beam epitaxy on GaAs(001) 2×4 surfaces in a wide range of compositions provided that a suitable strain relaxation profile is achieved within the ternary III–V buffer layer. We focus here on the structural properties of the resulting II–VI/III–V heterostructures and discuss the distribution of native defects, including misfit and threading dislocations, stacking faults, and surface corrugations. © *1998 American Vacuum Society*. [S0734-211X(98)05304-9]

I. INTRODUCTION

Heterovalent heterostructures, i.e., junctions comprised of semiconductors belonging to different families (e.g., II–VI/III–V or III–V/IV) have been attracting increasing attention in recent years for both basic and applied reasons.[1,2] On the fundamental side, the physics of these systems is in principle qualitatively different from that of the more conventional isovalent heterostructures.[1] Ideally abrupt heterovalent heterojunctions with polar orientation would be charged, and unstable.[3,4] Elimination of the resulting long-range electrostatic field may occur through the formation of point defects, which, in turn, may modify the band alignment. As far as applications are concerned, most materials currently being considered for optoelectronic devices in the short-wavelength visible range (e.g., the wide-gap II–VI materials or III–V nitrides) are grown on heterovalent substrates, and this emphasizes the importance of understanding and controlling the properties of heterovalent heterostructures.

Strain further complicates the issue, since the heterovalent substrates are seldom lattice matched to the active epilayers, and strain affects *per se* the electronic structure of the heterojunctions,[1,5] and may lead to the formation of extended as well as point defects.[1,5] Substantial progress towards the development of lattice-matched heterovalent heterostructures has been made in the II–VI/III–V area, in parallel with the recent demonstration of blue–green coherent emitters.[6] Because of the lack of II–VI substrates of suitable quality and doping, most such lasers have been fabricated by molecular beam epitaxy (MBE) on GaAs wafers. ZnSe, with a lattice parameter $a_0=5.6687$ Å,[7] exhibits a 0.27% in-plane mismatch with GaAs, but is lattice matched to $In_{0.038}Ga_{0.962}As$,[8] so several authors have attempted to achieve lattice-matched interfaces by incorporating $In_{0.04}Ga_{0.96}As$ buffer layers in blue–green lasers.[9,10]

We propose $Zn_{1-y}Cd_ySe/In_{1-x}Ga_xAs$ heterojunctions as a new prototype family of II–VI/III–V heterovalent heterojunctions that can be fabricated by MBE in lattice-matched form in a wide range of compositions on GaAs wafers, provided that a suitable strain-relaxation profile is achieved in the ternary III–V layers. We review here the conditions under which lattice matching is achieved, and the nature and spatial distribution of the dominant extended defects which are found in the structure.

An additional motivation of our work is the goal of eliminating strain from the active layer of current II–VI based blue–green lasers. $Zn_{1-y}Cd_ySe$ alloys are widely utilized as active layers in laser diodes grown on GaAs, and the large resulting compressive strain appears to promote device degradation.[11,12] Since high-quality $In_xGa_{1-x}As$ wafers with $x\geqslant0.02$ are not available because of homogeneity problems in high-x bulk crystals, fabrication of $In_xGa_{1-x}As$ buffer layers with optimized concentration and strain relaxation profile on GaAs seems at present the only viable option. We present here results for $Zn_{1-y}Cd_ySe/In_xGa_{1-x}As$ heterostructures of interest for both blue ($y=0$ and 0.15) and blue–green ($y\sim0.25$) emitters.

II. EXPERIMENTAL DETAILS

All heterostructures were grown by solid-source MBE in a system which includes interconnected chambers for the growth of II–VI and III–V materials and an analysis chamber with monochromatic x-ray photoemission spectroscopy (XPS) capabilities. After thermal removal of the native oxide

[a]Present address: Dept. of Physics, University of Illinois at Urbana-Champaign, Urbana, IL 61801.
[b]Also with Istituto ICMAT del CNR, Monterotondo, I-00016 Rome, Italy.
[c]Also with Dipartimento di Fisica, Universita' di Trieste, I-34127 Trieste, Italy and Dept. of Chemical Engineering and Materials Science, University of Minnesota, Minneapolis, MN 55455.
[d]Present address: Laboratorio Nazionale TASC-INFMe Sincrotrone Trieste S.C.p.A., Area di Ricerca Padriciano 99, I-34012 Trieste, Italy.

from semi-insulating GaAs(001) wafers, ~0.5-μm-thick GaAs buffer layers were initially grown at 600 °C. $In_xGa_{1-x}As$ epilayers 1–2 μm thick were subsequently grown at 490–500 °C with III/V beam pressure ratios (BPRs) in the 1/15–1/30 range, as determined from an ion gauge positioned at the sample location. Typical growth rates were between 1 and 1.3 μm/h. The indium content in the alloy was calibrated *in situ* by means of XPS, and *ex situ* by x-ray diffraction (XRD), photoluminescence (PL) spectroscopy, or Rutherford backscattering spectrometry (RBS).[13]

When required, graded composition $In_xGa_{1-x}As$ layers in which x was varied superlinearly with a parabolic composition profile were designed, as described in Sec. III, and fabricated by gradually increasing the indium cell temperature during growth. The composition profile of the graded layers was tested *a posteriori* by RBS and secondary ion mass spectrometry.

On the resulting $In_xGa_{1-x}As$ surface, $Zn_{1-y}Cd_ySe$ overlayers were deposited at 250–290 °C with a II/VI BPR of 1 or 0.4. Under the growth conditions employed the layers exhibited a $c(2\times2)$ (BPR=1) or (2×1) (BPR=0.4) surface reconstruction, as determined by reflection high energy electron diffraction (RHEED). The cadmium concentration in the alloy was also calibrated *in situ* by XPS and *ex situ* by RBS.

The extended defect density for each sample was probed using plan-view and cross-sectional transmission electron microscopy (TEM) micrographs. Thin foil samples were obtained by ion milling the structures at room temperature using 5 keV Ar^+ ions at an angle of incidence of 4° until perforation. Plan-view images obtained using a Philips EM430ST TEM operated at 300 keV allowed us to sample the overall heterostructure in sections as thick as 2 μm. Observations in thin regions of the plan-view thin foils allowed us to focus on the structural quality of the II–VI epilayer alone, while thicker regions yielded information on the whole sequence of epilayers down to the III–V buffer/substrate interface. Cross-sectional micrographs were recorded using either a JEOL 2000 FX TEM operated at 200 keV or a Philips EM430ST TEM operated at 300 keV.

The residual strain in the epilayers was determined either through XRD using a double-crystal diffractometer[14] or from the measured channeling directions using ^{4}He beams with an energy of 2.0 or 4.0 MeV.[13,15,16] Throughout this article the measured elastic deformation will be quantified in terms of the diagonal components of the strain tensor $\epsilon_{\parallel}$ and $\epsilon_{\perp}$.[17]

The surface morphology of the samples was examined using Nomarski optical microscopy and atomic force microscopy (AFM). The AFM images were obtained using a commercial instrument operated in contact mode with Si_3N_4 tips on cantilevers with a spring constant of 0.06–0.12 N/m, and typical scan rates in the 0.5–2.0 Hz range.

III. RESULTS AND DISCUSSION

A. Dislocations

In Table I we summarize the nominal parameters of $In_xGa_{1-x}As$ and $Zn_{1-y}Cd_ySe$ bulk alloys that would be lattice matched at room temperature for $y=0$, 0.15, and 0.25. The lattice parameters of the $Zn_{1-y}Cd_ySe$ alloys were obtained by linear interpolation between the lattice parameter of ZnSe (Ref. 18) and that measured in epitaxial, relaxed CdSe epilayers grown with a zinc blende structure on GaAs.[19] The lattice parameters of the $In_xGa_{1-x}As$ alloys were also obtained through interpolation from literature values.[20] The parallel decrease in the band gap with an increasing lattice parameter shown in Table I defines a series of potentially lattice-matched heterojunctions in which the band gap difference remains virtually unchanged while becoming an increasing fraction of the band gap of each semiconductor constituent. This should produce a substantial modulation of confinement effects in the heterostructure series.

TABLE I. Nominal parameters of $In_xGa_{1-x}As$ and $Zn_{1-y}Cd_ySe$ bulk alloys that would be lattice matched at room temperature for $y=0$, 0.15, and 0.25. Column 1: Lattice parameter; column 2: Cd content in the II–VI alloy; column 3: direct band gap of the II–VI alloy: column 4: In content in the III–V alloy; column 5: direct band gap of the III–V alloy; column 6: band gap difference between lattice-matched II–VI and III–V alloys.

	$Zn_{1-y}Cd_ySe$		$In_xGa_{1-y}As$		
a_0 (Å)	y	E_G (eV)	x	E_G (eV)	ΔE_G (eV)
5.669	0	2.70	0.04	1.38	1.32
5.730	0.15	2.55	0.19	1.22	1.33
5.771	0.25	2.44	0.29	1.11	1.33

Implementation of such lattice-matched heterostructures on GaAs wafers requires that controlled relaxation is obtained within $In_xGa_{1-x}As$ epilayers of a practical thickness (1–2 μm). For sufficiently low values of x this can be achieved using homogeneous composition layers. For example, in Fig. 1(a) we show a cross-sectional TEM micrograph of a $ZnSe/In_xGa_{1-x}As/GaAs$ heterostructure incorporating a 2-μm-thick ternary buffer layer with homogeneous composition $x=0.05$. At the interface between the ternary III–V layer and GaAs, an important dislocation network can be seen. However, these defects are confined near the interface, and no threading defects are observed within the $In_xGa_{1-x}As$ ternary layer or the ZnSe overlayer. From plan-view studies we estimate an upper limit of less than 2×10^4 cm^{-2} for the threading dislocation (TD) density in the II–VI overlayer.

When the mismatch between the II–VI/III–V heterostructure and the GaAs substrate becomes too high, homogeneous composition $In_xGa_{1-x}As$ layers become less suitable for the purpose. In Fig. 1(b) we show a cross-sectional TEM micrograph of a $Zn_{0.85}Cd_{0.15}Se/In_{0.19}Ga_{0.81}As/GaAs$ heterostructure incorporating a 300-nm-thick II–VI overlayer and a ~1-μm-thick, homogeneous composition $In_{0.19}Ga_{0.81}As$ layer. Although the vast majority of the misfit dislocations (MDs) are at the $In_xGa_{1-x}As/GaAs$ interface, the larger dislocation interaction, as compared to Fig. 1(a), is seen to be accompanied by the emergence of a number of TDs, which affect both the bulk of the ternary III–V layer and the II–VI over-

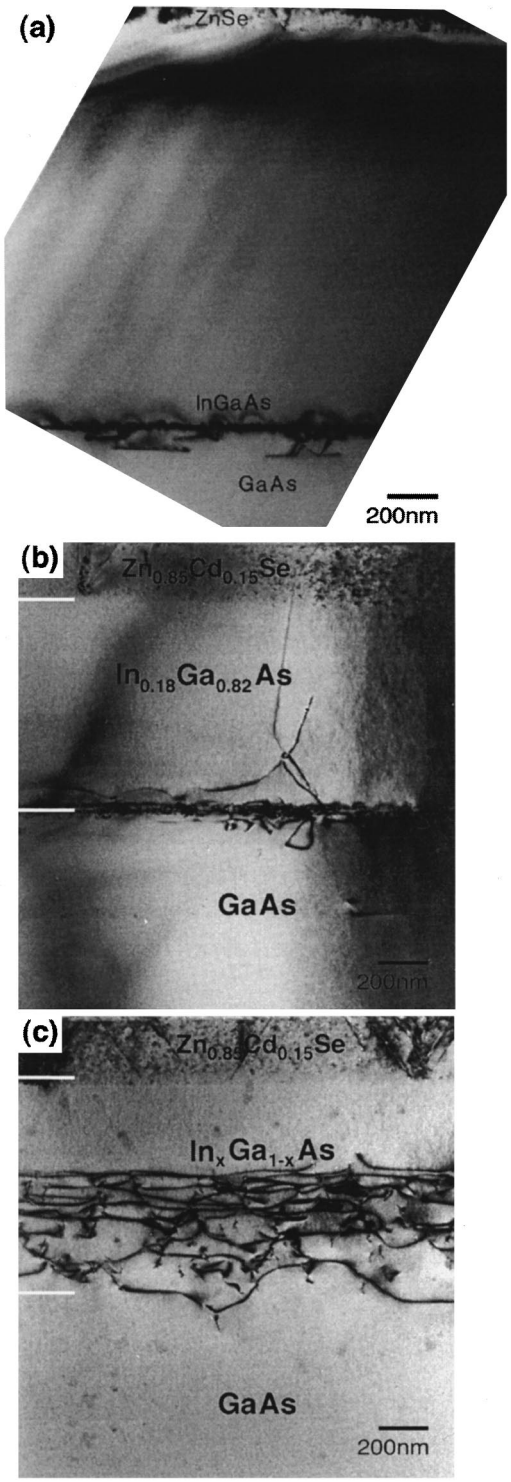

FIG. 1. (a) TEM micrograph of a $ZnSe/In_{0.05}Ga_{0.95}As/GaAs(001)$ heterostructure which includes a 100-nm-thick ZnSe epilayer and a 2-μm-thick, homogeneous composition $In_{0.05}Ga_{0.95}As$ layer. The cross-sectional image was obtained in two-beam diffraction conditions near the [110] zone axis. (b) Cross-sectional TEM micrograph of a $Zn_{0.85}Cd_{0.15}Se/In_{0.19}Ga_{0.81}As/GaAs$ heterostructure incorporating a 300-nm-thick II–VI overlayer and a $\sim$1-μm-thick, homogeneous composition $In_{0.19}Ga_{0.81}As$ layer. (c) Cross-sectional TEM micrograph of a $Zn_{0.85}Cd_{0.15}Se/In_xGa_{1-x}As/GaAs$ heterostructure incorporating a 300-nm-thick II–VI overlayer and a $\sim$1-μm-thick, graded composition $In_xGa_{1-x}As$ layer in which the In concentration exhibited a parabolic, superlinear profile from $x=0$ at the bottom to $x_0=0.23$ at the top.

layer. Dislocation interaction is known to enhance the nucleation of additional dislocations since the already-present threading segments are prevented from gliding further.[21]

To reduce the number of TDs and to avoid the three-dimensional (3D) growth effects which hinder fabrication of high-quality $In_xGa_{1-x}As$ layers with higher In concentrations on GaAs,[16,22,23] we employed $In_xGa_{1-x}As$ epilayers in which the In concentration was varied gradually from $x=0$ at the interface with the substrate to the desired $x=x_0$ at the surface, i.e., at the II–VI/III–V interface. As discussed elsewhere,[15,24] we selected a parabolic, superlinear concentration profile:

$$x(t)=x_0\left[1-\left(1-\frac{t}{T}\right)^2\right], \tag{1}$$

where t it the distance from the GaAs substrate and T is the total thickness of the $In_xGa_{1-x}As$ layer. The profile in Eq. (1) was selected for its simplicity, relatively flat behavior in the near-surface region, which makes it less sensitive than other profiles to variations in composition and layer thickness, and for its expected property of confining MDs away from the surface while minimizing dislocation interaction.[24]

The corresponding residual strain at the film surface in the direction parallel to the interface $\epsilon_\parallel$ (Ref. 17) can be calculated from the following expression obtained through a semiempirical model of strain relaxation:[24,25]

$$\epsilon_\parallel^5=\left(\frac{9K}{4}\right)^2\frac{x_0}{T^2}\left(\frac{a_0(\mathrm{InAs})}{a_0(\mathrm{GaAs})}-1\right), \tag{2}$$

where $K=0.0037\pm0.0007$ nm is an empirical constant, and a_0 (InAs) and a_0 (GaAs) are the equilibrium (unstrained) lattice parameters of the binary parent compounds. Based on the predictions of Eq. (2), the In concentration x_0 at the surface of the graded layer must exceed the values of x in Table I to compensate for the partial character of the strain relaxation within any layer of finite-size thickness. For example, in order to obtain a surface lattice parameter[17] that matches that of a bulk $Zn_{0.85}Cd_{0.15}Se$ alloy using an $In_xGa_{1-x}As$ graded layer with $T=1100$ nm, the surface composition should be $x_0=0.245$.

In Fig. 1(c) we show a cross-sectional TEM micrograph of a $Zn_{0.85}Cd_{0.15}Se/In_xGa_{1-x}As/GaAs$ heterostructure incorporating a 300-nm-thick II–VI overlayer and a $\sim$1-μm-thick, graded composition $In_xGa_{1-x}As$ layer in which the In concentration exhibited a parabolic, superlinear profile of Eq. (1) from $x=0$ at the bottom to $x_0=0.23$ at the top. MDs are seen to be distributed throughout a region approximately 500 nm wide, gradually relaxing most of the misfit within this region, and leaving the remaining portion of the buffer unaffected, in agreement with theoretical predictions.[24–26] Within our experimental sensitivity, no TDs are observed.

The $Zn_{1-y}Cd_ySeSe/In_xGa_{1-x}As$ heterostructures discussed in what follows will include homogeneous composition ternary III–V layers only for $y=0$, while samples with $y=0.15$ and 0.25 will always be implemented using graded composition $In_xGa_{1-x}As$ layers with target structural parameters derived from Eqs. (1) and (2).

TABLE II. Experimental structural and compositional parameters of $Zn_{1-y}Cd_ySe/In_xGa_{1-x}As$ heterostructures grown by MBE on GaAs(001) substrates. The data in the first row ($y=0$) were obtained from XRD. The data in the second and third rows were obtained from RBS and channeling studies. Column 1: Cd content in the II–VI overlayer; column 2: in-plane strain within the II–VI overlayer; column 3: In content in the near-surface region of the III–V layer; column 4: in-plane residual strain in the near-surface region of the III–V layer; column 5: type and thickness of the $In_xGa_{1-x}As$ layer employed. The *h* and *g* labels denote homogeneous and graded composition layers, respectively.

$Zn_{1-y}Cd_ySe$		$In_xGa_{1-x}As$		
y	$\epsilon_\parallel$ (%)	x_0	$\epsilon_\parallel$ (%)	Type/thickness (nm)
0	-0.014 ± 0.007	0.051 ± 0.002	-0.097 ± 0.016	h/2000
0.150 ± 0.04	-0.29 ± 0.04	0.214 ± 0.004	-0.40 ± 0.04	g/920
0.249 ± 0.002	-0.14 ± 0.04	0.340 ± 0.004	-0.48 ± 0.04	g/915

In Fig. 1 no MDs are observed within the experimental sensitivity at any of the II–VI/III–V interfaces, indicating that the II–VI overlayers grow pseudomorphically on the III–V layers. To quantify how close a lattice–match was routinely achieved, we list in Table II the structural parameters measured for three $Zn_{1-y}Cd_ySeSe/In_xGa_{1-x}As$ heterostructures with $y=0$, 0.15, and 0.25. To obtain structural information on both the II–VI overlayer and the near-surface region of the graded composition III–V epilayer within the *same* heterostructure, we followed a two-step growth process. First, a graded III–V ternary epilayer was grown on a suitable GaAs wafer and protected with an As cap layer. The wafer was then removed from the MBE system and cleaved into different sections. Some sections were used in RBS studies of composition and strain. Others were introduced again in the MBE system and used as substrates for $Zn_{1-y}Cd_ySe$ growth after thermal removal of the As cap layer. In view of the RBS sampling depth and the relatively flat profile in the near-surface region [see Eq. (1)], the RBS-derived values of x will be taken as experimental determinations of the surface composition x_0.

The structural parameters of the $In_xGa_{1-x}As$ layers in Table II indicate that a substantial amount of residual strain is present in the III–V layers, as expected because of the finite thickness of any practical ternary buffer layer. For the graded composition layers, the experimental values of $\epsilon_\parallel$ (-0.40% and -0.48%) are very similar to the theoretical predictions (-0.42% and -0.46%, respectively) obtained from Eq. (2) using the experimental values of x_0 and T. The implication is that the semi-empirical model[15,24,25] does remarkably well in predicting the strain relaxation in the graded layers. The target values of x_0 and T (i.e., those required for lattice match to the II–VI overlayer) are achieved within 5%–10% through the growth procedure employed, with a trend toward lower thicknesses (by up to 10% of the target T) and lower In concentrations (by up 2%–5% of the target x_0) as compared to the optimum design values.

The structural parameters of the II–VI overlayers in Table II indicate that they grow pseudomorphically on the III–V epilayers, so that the strain present largely reflects the deviations of the ternary III–V parameters from the design values. For the $ZnSe/In_xGa_{1-x}As$ heterostructure, the low strain achieved ($\epsilon_\parallel=-0.014\%\pm0.007\%$) indicates that the excess In concentration over the value in Table I (5% as opposed to 4%) compensates almost exactly for the partial character of the strain relaxation within the III–V layer. The resulting expected critical thickness for the II–VI overlayer exceeds 300 μm,[14] suggesting that for all practical purposes lattice matching has been achieved.

The strain in the II–VI overlayer is somewhat larger for $Zn_{0.85}Cd_{0.15}Se/In_xGa_{1-x}As$ and $Zn_{0.75}Cd_{0.25}Se/In_xGa_{1-x}As$ heterostructures, reflecting the larger deviations of the ternary III–V parameters from the design values in the graded-composition layers. To put these results in perspective, two points should be noted: (i) Table II was compiled using a subset of samples for which RBS studies were performed on both the III–V and the II–VI layers, and are not necessarily those for which the best lattice matching was achieved. For example, on a total set of six $Zn_{1-y}Cd_ySe/In_xGa_{1-x}As$ heterostructures with $y=0.15-0.25$, the minimum strain encountered in the II–VI overlayer was -0.06% and the maximum -0.29%. (ii) The lattice matching achieved should be assessed vis-à-vis the applications envisioned. For example, the mismatch between $Zn_{0.75}Cd_{0.25}Se$ and GaAs is 2.0%, so that a -2.0% strain exists in the active layer of any corresponding blue–green laser fabricated on GaAs. If the same laser were to be fabricated on the corresponding graded layer in Table II, the strain would be decreased by a factor of 14.3.

In the absence of MDs and TDs in the II–VI epilayers, the main type of extended defect that remains is native stacking faults on {111} planes. Several such defects are clearly observed in Fig. 1, giving rise to the characteristic type of V-shaped contrast in the cross-sectional image. Stacking faults are known to form at the II–VI/III–V interface and to propagate upward during growth along {111} fault planes. Although some isolated Frank stacking faults exist on (111) and $(\bar{1}\bar{1}\bar{1})$ fault planes, we have shown[27,28] that the majority of such defects are Shockley stacking fault pairs on (111) and $(\bar{1}\bar{1}\bar{1})$ fault planes, bounded by partial dislocations exhibiting Burgers vectors (1/6)$[1\bar{2}1]$ and (1/6)[211] for the former, and (1/6)[211] and (1/6)$[1\bar{2}1]$ for the latter.

A discussion of the stacking fault issue, together with a review of the extensive recent literature on this subject, can be found elsewhere.[27,28] Here we remind the reader that in view of the presence of the partial dislocations bounding the

stacking faults, the II–VI overlayers in Fig. 1 cannot be considered, strictly speaking, dislocation free. However, such stacking faults do not contribute significantly to strain relaxation, and in any case their concentration can be reduced below 10^4 cm^{-2} by controlling the interface nucleation stage, either by acting on the Zn/Se BPR (Se-rich growth conditions yield lower stacking fault densities[27,28]) or by predosing the surface with submonolayer coverages of Zn.[29,30]

B. Surface properties

Figure 2 shows the surface morphology of the three types of $Zn_{1-y}Cd_ySe/In_xGa_{1-x}As$ heterostructures examined in this study as sampled by Nomarski optical microscopy. Clearly visible in all three cases is a regular pattern of parallel lines on the surface with a separation of approximately 1 μm. These striations run throughout the sample along the [110] direction. Weaker lines are also visible in the [110] perpendicular surface direction, with lower density and therefore larger spacing yielding a characteristic cross-hatched pattern.

Nomarski optical micrographs of the corresponding III–V buffer layers can be found elsewhere[14–16] and are not reproduced here for sake of brevity. The similarity of the cross-hatched patterns from the II–VI overlayers and the III–V substrates, and the fact that the striations are absent from the surface of pseudomorphic ZnSe layers grown on GaAs[14] suggest that the surface morphology of the $Zn_{1-y}Cd_ySe$ overlayers replicates that of the underlying $In_xGa_{1-x}As$ epilayers.

Surface corrugations arranged to give a cross-hatched pattern have been observed for both $In_xGa_{1-x}As$ epilayers[31–33] as well for as $Si_{1-x}Ge_x$ epilayers[21,34] during growth on lattice-mismatched substrates when the critical thickness was exceeded. In general, their origin has been phenomenologically related to the misfit dislocation network at the epilayer–substrate interface,[31] based on their orientation, and on the fact that they were not observed in layers which do not contain substantial numbers of glissile misfit dislocations.[31]

The similar orientation of the surface cross-hatched pattern and the MD dislocation network near the $In_xGa_{1-x}As/GaAs$ is illustrated by a comparison of the results of Fig. 2 with selected plan-view TEM micrographs in Fig. 3. In Fig. 3(a) we show the MD network observed in a $ZnSe/In_xGa_{1-x}As(001)$ heterostructure incorporating a 300-nm-thick II–VI overlayer and a 2-μm-thick $In_xGa_{1-x}As$ layer with homogeneous composition $x=0.043$. Figure 3(b) depicts the corresponding MD network in a $Zn_{0.75}Cd_{0.25}Se/In_xGa_{1-x}As(001)$ heterostructure incorporating a 300-nm-thick II–VI overlayer and a $\sim$1-μm-thick $In_xGa_{1-x}As$ layer with graded composition profile and surface composition $x_0=0.33$.

In both micrographs, a relatively ordered, asymmetric network of misfit dislocations is observed. Most of the MDs are found to be mixed dislocations with Burgers vectors of the $a/2\langle 110\rangle$ type, at 60° to the dislocation line.[15,35] The dislocation lines appear as straight lines in the micrographs because they lie at the intersection of {111} slip planes with the (001) heterointerface and are in [110] and [$\bar{1}$10] directions. The apparent asymmetry in the contrast associated with the network stems from the fact that along one of the two orthogonal $\langle 110\rangle$ directions, the dislocations are more uniformly distributed, while in the other there is a marked tendency for periodic bunching. This was attributed[15,35] to the different velocities of group III and group V dislocations in the zinc blende structure.[36]

The difference in the overall number of MD density be-

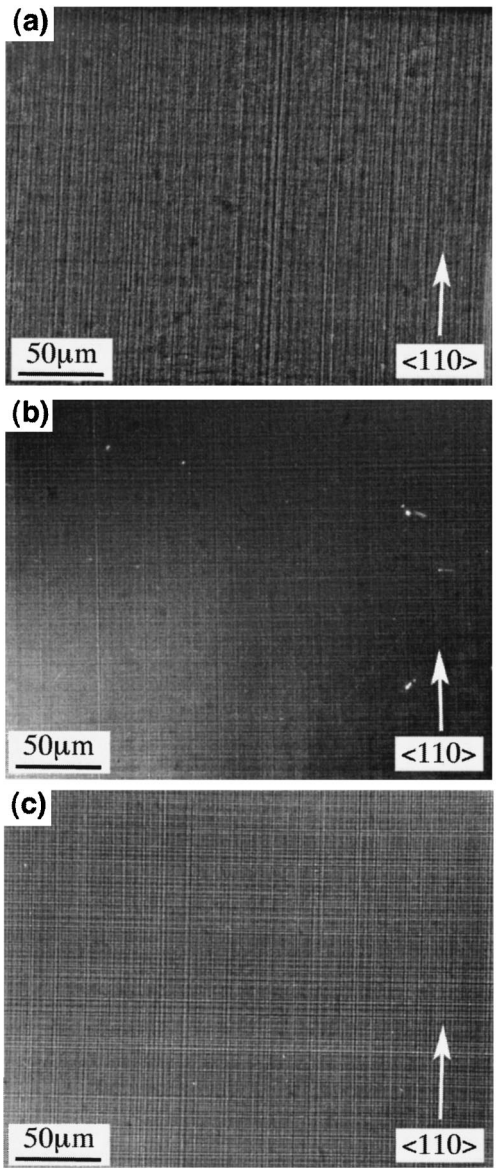

FIG. 2. (a) Surface morphology of a $ZnSe/In_xGa_{1-x}As(001)$ heterostructure grown on GaAs incorporating a 300-nm-thick II–VI overlayer and a 2-μm-thick $In_xGa_{1-x}As$ layer with homogeneous composition $x=0.043$, as measured with a Nomarski optical microscope. (b) Surface morphology of a $Zn_{0.85}Cd_{0.15}Se/In_xGa_{1-x}As(001)$ heterostructure incorporating a 300-nm-thick II–VI overlayer and a $\sim$1-μm-thick $In_xGa_{1-x}As$ layer with a graded composition profile and surface composition $x_0=0.23$. (c) Surface morphology of a $Zn_{0.75}Cd_{0.25}Se/In_xGa_{1-x}As(001)$ heterostructure incorporating a 300-nm-thick II–VI overlayer and a $\sim$1-μm-thick $In_xGa_{1-x}As$ layer with a graded composition profile and surface composition $x_0=0.33$.

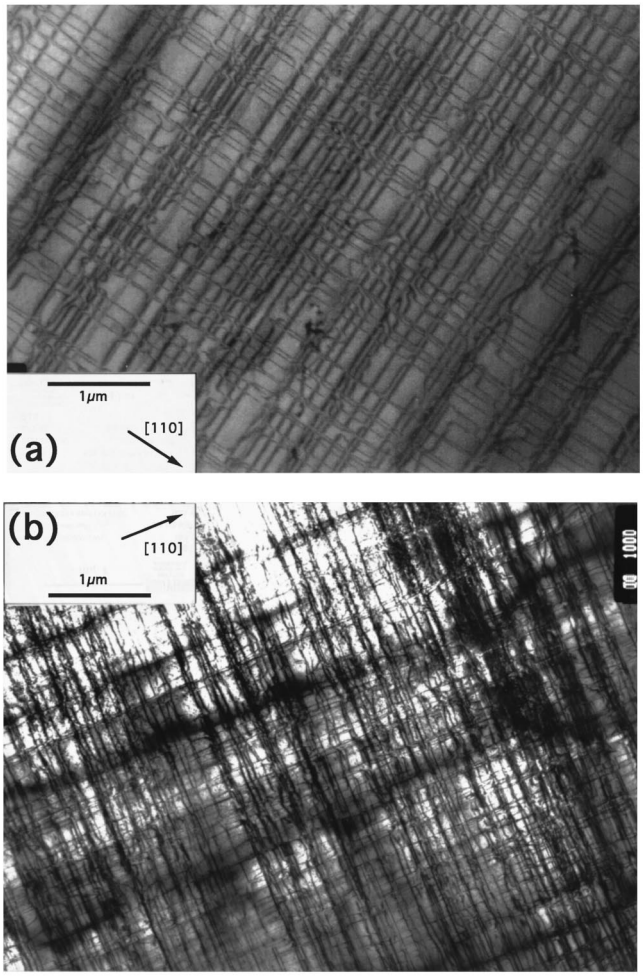

FIG. 3. TEM plan-view micrographs of $Zn_{1-y}Cd_ySe/In_xGa_{1-x}As$ heterostructures grown on GaAs, emphasizing the MD dislocation network near the $In_xGa_{1-x}As/GaAs$ interface. (a) $ZnSe/In_xGa_{1-x}As(001)$ heterostructure incorporating a 300-nm-thick II–VI overlayer and a 2-μm-thick $In_xGa_{1-x}As$ layer with homogeneous composition $x=0.043$. (b) $Zn_{0.75}Cd_{0.25}Se/In_xGa_{1-x}As(001)$ heterostructure incorporating a 300-nm-thick II–VI overlayer and a $\sim$1-μm-thick $In_xGa_{1-x}As$ layer with a graded composition profile and surface composition $x_0=0.33$.

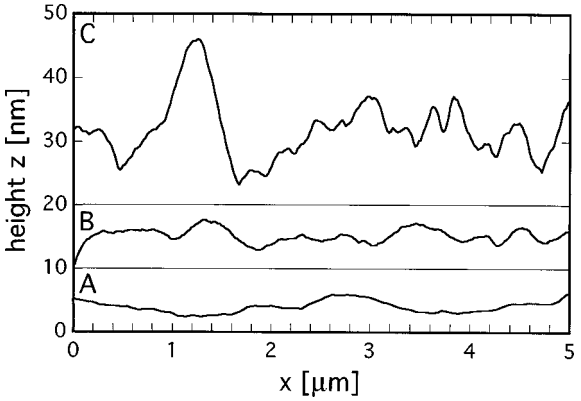

FIG. 4. AFM line scans for the type of samples depicted in Figs. 1 and 2, recorded in the direction perpendicular to the major surface corrugations, i.e., the [110] direction. (a) $ZnSe/In_xGa_{1-x}As(001)$ heterostructure grown on GaAs incorporating a 300-nm-thick II–VI overlayer and a 2-μm-thick $In_xGa_{1-x}As$ layer with homogeneous composition $x=0.043$. (b) $Zn_{0.85}Cd_{0.15}Se/In_xGa_{1-x}As(001)$ heterostructure incorporating a 300-nm-thick II–VI overlayer and a $\sim$1-μm-thick $In_xGa_{1-x}As$ layer with a graded composition profile and surface composition $x_0=0.23$. (c) $Zn_{0.75}Cd_{0.25}Se/In_xGa_{1-x}As(001)$ heterostructure incorporating a 300-nm-thick II–VI overlayer and a $\sim$1-μm-thick $In_xGa_{1-x}As$ layer with a graded composition profile and surface composition $x_0=0.33$.

tween Figs. 3(a) and 3(b) is simply a manifestation of the different lattice mismatch with the GaAs wafer, which is 0.27% for the sample in Fig. 3(a) and 2.0% for the sample in Fig. 3(b), yielding a 7.4-fold increase in the areal dislocation density. We emphasize, however, that while in the former case all of the dislocations are at the interface between the homogeneous composition ternary layer and the GaAs substrate [see the corresponding cross-sectional image in Fig. 1(a)], in the latter the larger number of MDs are distributed within a $\sim$500-nm-thick region of the ternary layer due to the graded concentration profile.

A more quantitative analysis of the surface corrugations for the three heterostructures in Fig. 2 was performed by AFM. In Fig. 4 we show line scans recorded in the direction perpendicular to the main corrugations, i.e., along the [110] direction. The line profile in Fig. 4(a) was obtained from a $ZnSe/In_xGa_{1-x}As(001)$ heterostructure grown on GaAs incorporating a 300-nm-thick II–VI overlayer and a 2-μm-thick $In_xGa_{1-x}As$ layer with homogeneous composition $x=0.043$. The amplitude of the corrugations is of the order of 3 nm, and the period larger than 1 μm. A more precise determination of the period as an average over several line scans from different regions of the same sample would yield 1.4 ± 0.4 μm.[14] The measured root mean square (rms) roughness of the surface is of the order of 1 nm.

The line scan in Fig. 4(b) was recorded from a $Zn_{0.85}Cd_{0.15}Se/In_xGa_{1-x}As(001)$ heterostructure incorporating a 300-nm-thick II–VI overlayer and a $\sim$1-μm-thick $In_xGa_{1-x}As$ layer with a graded composition profile and surface composition $x_0=0.23$. The amplitude of the corrugations is still of the order of 4–5 nm, but the period decreases to about 0.5 μm. Correspondingly, the rms roughness of the surface is 1.7 ± 0.4 nm.[15] The line profile in Fig. 4(c) was obtained from a $Zn_{0.75}Cd_{0.25}Se/In_xGa_{1-x}As(001)$ heterostructure incorporating a 300-nm-thick II–VI overlayer and a $\sim$1-μm-thick $In_xGa_{1-x}As$ layer with a graded composition profile and surface composition $x_0=0.33$. The amplitude of the corrugations is of the order of 10 nm, and the period 0.3–0.5 μm. Correspondingly, the rms roughness of the surface is of the order of 5 nm.[16] Much higher values of surface roughness are observed for heterostructures incorporating homogeneous as opposed to graded composition $In_xGa_{1-x}As$ layers, despite the lower value of the In concentration at the surface of the ternary III–V layer.[14–16]

C. Relation between dislocations and surface morphology

In general, the formation of a MD network is explained with one of two types of mechanisms. One mechanism[35] assumes that a number of TDs derive from an imperfect sub-

strate or from surface inhomogeneities of the substrate. In the presence of a misfit between the epilayer and substrate the TD lines are bent by the stress field within the film. TD segments confined at the interface would generate the necessary MDs. This is an efficient mechanism of strain relief which does not require the nucleation of new dislocations. However, since the $In_xGa_{1-x}As$ layers in the heterostructures under consideration contain a negligible TD density, we suggest that the second type of mechanism is dominant in our case.

In this alternate picture,[37,38] dislocation loops (DLs) starting at the surface of the growing film may expand by gliding along a {111} plane and provide the MD as they reach the interface, together with a pair of TDs which are annihilated upon reaching the edge of the epilayer. This implies two consequences: (i) Every MD at the interface would correspond to a monoatomic slip step on the epilayer surface. The direction of the step (arbitrary labeled up or down) would depend on the glide plane ({111} or $\{\bar{1}11\}$) and thus on the Burgers vector of the dislocation line ($a/2\langle 101\rangle$ or $a/2\langle 011\rangle$); (ii) dislocations with $a/2\langle 101\rangle$-type Burgers vectors contain a vertical component which produces a small tilt in the epilayer relative to the substrate. The existence of a small epilayer tilt is well established in literature,[39] and is especially important for $In_xGa_{1-x}As$ layers grown on misoriented substrates.[40] Bauer and co-workers observed both slip steps correlated to interface dislocations and a finite epilayer tilt in a recent scanning tunneling microscopy study of strained EuTe layers on PbTe.[41]

With such considerations in mind, we can explore a possible quantitative correlation between dislocation slip steps and surface corrugations. The average spacing between dislocation lines in our $In_{0.05}Ga_{0.95}As$ buffers was of the order of 100 nm [112 ± 7 nm for the sample in Fig. 3(a)]. Our AFM measurements yielded an average spacing of the major surface corrugations of approximately 1.5 μm [1.38 ± 0.4 μm for the sample in Fig. 4(a)]. This gives about 15 dislocations and slip steps per crossed-hatch period. Assuming a series of 7–8 ''up'' steps followed by 7–8 ''down'' steps per period, and a monoatomic step height of 0.28 nm, we estimate a height modulation of 2.1 nm, i.e., of the same order of magnitude as that observed in Fig. 4(a).[14]

The presence of series of up steps and down steps rather than a random distribution is not predicted *a priori* by the DL mechanism. None of the {111} gliding planes is *a priori* preferred so that MDs with $a/2\langle 101\rangle$ or $a/2\langle 011\rangle$ Burgers vectors, and hence the up and down steps on the surface, should be distributed randomly. DLs, however, are not the only MD nucleation sources once the dislocation density becomes high enough for effective interaction between MD lines to take place.

For example, Hagen and Strunk[42] proposed that the repulsive interaction between two dislocations with the same Burgers vector and crossed dislocation lines along the [011] and $[0\bar{1}1]$ directions would generate a right angle and a rounded right angle segment. The latter can act as a starting point for a new MD line with the *same* Burgers vector.[43] Following the glide along a {111} plane, a slip step at the surface is generated, but since the Burgers vector remains the same, the direction of the steps (up or down) also remains the same. So the original random distribution of MDs originating from the DL mechanism, followed by MD multiplication to generate bunches of MDs with the same Burgers vectors would account for the observed surface morphology through a purely plastic mechanism.

The above picture readily explains the smoother surface morphology of heterostructures incorporating a graded as opposed to a homogeneous composition $In_xGa_{1-x}As$ layer, since in the graded layers the spacing of the dislocation lines in the direction perpendicular to the interface is much larger than in the homogeneous composition buffer, greatly reducing the importance of the MD multiplication mechanism. Qualitatively, the reduced dislocation interaction in the graded buffer may explain why the roughness of the surface depicted in Fig. 4(b) is still of the same order of magnitude as that depicted in Fig. 4(a) despite the threefold increase in lattice mismatch.

IV. CONCLUSIONS

We have determined growth protocols and design parameters for the implementation of lattice-matched heterovalent $Zn_{1-y}Cd_ySe/In_xGa_{1-x}As$ heterostructures on GaAs(100) in the composition range of interest for blue–green optoelectronic applications ($0<y<0.3$). Except for the smallest Cd and In concentrations explored, minimization of the threading dislocation density and surface roughness requires the use of graded composition III–V ternary layers. In all cases, the In concentration within the III–V ternary layer has to be selected so that the partial character of strain relaxation is appropriately compensated. Final strains at or below the 0.1% level for the II–VI epilayers are routinely achieved by molecular beam epitaxy.

The resulting II–VI epilayers are dislocation free, except for the partial Frank and Shockley dislocations bounding the stacking faults originating at the II–VI/III–V interface. The surface morphology of the II–VI overlayers is found to exhibit a crossed-hatch pattern of surface corrugations with amplitudes in the 3–10 nm range and periods of 0.3–1.5 μm. Its origin maybe purely plastic, and follow from the formation of slip steps at the surface during dislocation multiplication at the epilayer–substrate interface.

ACKNOWLEDGMENTS

This work was supported in part by the Consiglio Nazionale delle Ricerche of Italy under the MADESS project and by the Commission of the European Communities. The authors thank G. Bauer, R. Cingolani, M. Lomascolo, and Y. Zhuang for useful discussions and for providing them with their results prior to publication.

[1]A. Franciosi and C. G. Van de Walle, Surf. Sci. Rep. **25**, 1 (1996).
[2]L. J. Brillson, in *Handbook on Semiconductors*, edited by P. T. Landsberg (North-Holland, Amsterdam, 1992), Vol. I, p. 281.

[3]W. Harrison, J. Vac. Sci. Technol. **16**, 1492 (1979); K. Kunc and R. M. Martin, Phys. Rev. B **24**, 3445 (1981); R. G. Dandrea, S. Froyen, and A. Zunger, *ibid.* **42**, 3213 (1990).
[4]S. Baroni, R. Resta, and A. Baldereschi, in *Proceedings of the XIX International Conference on the Physics of Semiconductors*, edited by W. Zawadzki (Institute of Physics, Polish Academy of Sciences, Wroclaw, 1988), p. 525; M. Peressi, S. Baroni, R. Resta, and A. Baldereschi, Phys. Rev. B **43**, 7347 (1991).
[5]J. Tersoff and C. G. Van de Walle, Phys. Rev. Lett. **59**, 946 (1987); R. G. Dandrea and C. B. Duke, J. Vac. Sci. Technol. B **11**, 1553 (1993).
[6]See, for example, Proc. SPIE **2346**, 1 (1994).
[7]J. Petruzzello, B. L. Greenberg, D. A. Cammack, and R. Dalby, J. Appl. Phys. **63**, 2299 (1988).
[8]S. Adachi, J. Appl. Phys. **53**, 8775 (1982).
[9]H. Jeon, J. Ding, A. V. Nurmikko, H. Luo, N. Samarth, J. K. Furdyna, W. A. Bonner, and R. E. Nahory, Appl. Phys. Lett. **57**, 2413 (1990); W. Xie, D. C. Grillo, R. L. Gunshor, M. Kobayashi, H. Jeon, J. Ding, A. V. Nurmikko, G. C. Hua, and N. Otsuka, *ibid.* **60**, 1999 (1992); H. Jeon, J. Ding, A. V. Nurmikko, W. Xie, D. C. Grillo, M. Kobayashi, R. L. Gunshor, G. C. Hua, and N. Otsuka, *ibid.* **60**, 2045 (1992).
[10]D. Hervé, R. Accomo, E. Molva, L. Vanzetti, J. J. Paggel, L. Sorba, and A. Franciosi, Appl. Phys. Lett. **67**, 2144 (1995).
[11]D. Herve, J. M. Bonard, L. Vanzetti, J. J. Paggel, L. Sorba, J. D. Ganiere, E. Molva, and A. Franciosi, J. Cryst. Growth **159**, 600 (1996).
[12]J.-M. Bonard, J.-D. Ganiere, L. Vanzetti, J. J. Paggel, L. Sorba, A. Franciosi, D. Herve, and E. Molva, J. Appl. Phys. **83**, 1945 (1998).
[13]A. V. Drigo, Mikrochim. Acta **114–115**, 89 (1994); A. Armigliato, M. Servidori, F. Cembali, R. Fabbri, R. Rosa, F. Corticelli, D. Govoni, A. V. Drigo, M. Mazzer, F. Romanato, S. Frabboni, R. Balboni, S. S. Iyer, and A. Guerrieri, Microsc. Microanal. Microstruct. **3**, 363 (1992).
[14]S. Heun, J. J. Paggel, L. Sorba, S. Rubini, A. Bonanni, R. Lantier, M. Lazzarino, B. Bonnani, A. Franciosi, J.-M. Bonard, J.-D. Ganiere, Y. Zhuang, and G. Bauer, J. Appl. Phys. **83**, 2504 (1998).
[15]B. H. Müller, R. Lantier, L. Sorba, S. Heun, S. Rubini, M. Lazzarino, A. Franciosi, E. Napolitani, F. Romanato, A. Drigo, L. Lazzarini, and G. Salviati (unpublished).
[16]B. H. Müller, R. Lantier, L. Sorba, S. Rubini, M. Lazzarino, S. Heun, A. Bonanni, G. Bratina, A. Franciosi, E. Napolitano, F. Romanato, and A. Drigo, J. Cryst. Growth **185**, 21 (1998).
[17]It is, therefore, $\epsilon_{\parallel}=(a_{\parallel}-a_0)/a_0$, $\epsilon_{\perp}=(a_{\perp}-a_0)/a_0$, where $a_{\parallel}$ and $a_{\perp}$ are the measured lattice parameters in the directions parallel and perpendicular to the interface, respectively, and a_0 is the equilibrium (unstrained) lattice parameter. In a biaxial strain field the two values are connected by the simple relations, $\epsilon_{\perp}=-\alpha\epsilon_{\parallel}$, $\alpha=2(C_{12}/C_{11})=2(\nu/1-\nu)$, where C_{12} and C_{11} are the elastic stiffness constants and ν is Poisson's ratio.
[18]J. Petruzzello, B. L. Greenberg, D. A. Cammack, and R. Dalby, J. Appl. Phys. **63**, 2299 (1988).
[19]N. Samarth, H. Lou, J. K. Furdyna, S. B. Qudri, Y. R. Lee, A. V. Ramdas, and N. Otsuka, Appl. Phys. Lett. **54**, 2680 (1989). These authors also reported a direct band gap of 1.67 eV at 300 K.
[20]*Semiconductors—Group IV Elements and III–V Compounds*, edited by O. Madelung, Data in Science and Technology Series (Springer, Berlin, 1991).
[21]E. A. Fitzgerald, Y. H. Xie, M. L. Green, D. Brasen, A. R. Kortan, J. Michel, Y. J. Mii, and B. E. Weir, Appl. Phys. Lett. **59**, 811 (1991).
[22]S. Guha, A. Madhukar, and K. J. Rajkumar, Appl. Phys. Lett. **57**, 2110 (1990).
[23]J. M. Moison, F. Houzay, F. Barthe, L. Leprince, E. Andre', and O. Vatel, Appl. Phys. Lett. **64**, 196 (1994), and references therein.
[24]A. Bosacchi, A. C. De Riccardis, P. Frigeri, S. Franchi, C. Ferrari, S. Gennari, L. Nasi, G. Salviati, A. V. Drigo, and F. Romanato, J. Cryst. Growth **175/176**, 1009 (1997); L. Lazzarini, C. Ferrari, S. Gennari, A. Bosacchi, S. Franchi, F. Romanato, M. Berti, A. V. Drigo, and G. Salviati, Inst. Phys. Conf. Ser. **157**, 149 (1997).
[25]A. V. Drigo, A. Aydinli, A. Carnera, F. Genova, C. Rigo, C. Ferrari, P. Franzosi, and G. Salviati, J. Appl. Phys. **66**, 1975 (1989).
[26]J. Tersoff, Appl. Phys. Lett. **62**, 693 (1993).
[27]S. Heun, J. J. Paggel, S. Rubini, L. Sorba, A. Franciosi, J.-M. Bonard, and J.-D. Ganiere, Appl. Phys. Lett. **70**, 237 (1997); S. Heun, J. J. Paggel, L. Sorba, S. Rubini, A. Franciosi, J.-M. Bonard, and J.-D. Ganiere, J. Vac. Sci. Technol. B **15**, 1279 (1997).
[28]J.-M. Bonard, J.-D. Ganiere, S. Heun, J. J. Paggel, S. Rubini, L. Sorba, and A. Franciosi, Philos. Mag. Lett. **75**, 219 (1997).
[29]B. J. Wu, G. M. Haugen, J. M. DePuydt, L. H. Kuo, and L. Salamanca-Riba, Appl. Phys. Lett. **68**, 2828 (1996).
[30]L. H. Kuo, K. Kimura, S. Miwa, Y. Yasuda, and T. Yao, Appl. Phys. Lett. **69**, 1408 (1996); L. H. Kuo, K. Kimura, Y. Yasuda, S. Miwa, C. G. Jin, K. Tanaka, and T. Yao, *ibid.* **68**, 2413 (1996).
[31]R. Beanland, M. Aindow, T. B. Joyce, P. Kidd, M. Lourenço, and P. J. Goodhew, J. Cryst. Growth **149**, 1 (1995).
[32]K. H. Chang, R. Gibala, D. J. Srolovitz, P. K. Bhattacharya, and J. F. Mansfield, J. Appl. Phys. **67**, 4093 (1990).
[33]S. F. Yoon, J. Vac. Sci. Technol. B **11**, 562 (1993).
[34]S. Y. Shiryaev, F. Jensen, and J. W. Petersen, Appl. Phys. Lett. **64**, 3305 (1994).
[35]J.-M. Bonard, Ph.D. thesis, Ecole Polytechnique Fédérale de Lausanne, Switzerland, 1996.
[36]M. S. Abrahams, J. Blanc, and C. J. Buiocchi, Appl. Phys. Lett. **21**, 185 (1972).
[37]J. W. Matthews, J. Vac. Sci. Technol. **12**, 126 (1975).
[38]J. W. Matthews, A. E. Blakeslee, and S. Mader, Thin Solid Films **33**, 253 (1976).
[39]J. M. Kang, C. S. Son, M.-S. Kim, Y. Kim, S.-K. Kim, and C. S. Kim, Appl. Phys. Lett. **67**, 641 (1995).
[40]F. Riesz, J. Cryst. Growth **140**, 213 (1994).
[41]G. Springholz, G. Bauer, and V. Holy, Surf. Sci. **365**, 453 (1996).
[42]W. Hagen and H. Strunk, Appl. Phys. **17**, 85 (1978).
[43]E. A. Fitzgerald, G. P. Watson, R. E. Proano, D. G. Ast, P. D. Kirchner, G. D. Pettit, and J. M. Woodall, J. Appl. Phys. **65**, 2220 (1989).